



# ELECTRON AND PHOTON - MATTER INTERACTION : ENERGY DISSIPATION AND INJECTION LEVEL

E. Napchan

► **To cite this version:**

E. Napchan. ELECTRON AND PHOTON - MATTER INTERACTION : ENERGY DISSIPATION AND INJECTION LEVEL. Journal de Physique Colloques, 1989, 50 (C6), pp.C6-15-C6-29. <10.1051/jphyscol:1989602>. <jpa-00229633>

**HAL Id: jpa-00229633**

**<https://hal.archives-ouvertes.fr/jpa-00229633>**

Submitted on 1 Jan 1989

**HAL** is a multi-disciplinary open access archive for the deposit and dissemination of scientific research documents, whether they are published or not. The documents may come from teaching and research institutions in France or abroad, or from public or private research centers.

L'archive ouverte pluridisciplinaire **HAL**, est destinée au dépôt et à la diffusion de documents scientifiques de niveau recherche, publiés ou non, émanant des établissements d'enseignement et de recherche français ou étrangers, des laboratoires publics ou privés.

**ELECTRON AND PHOTON - MATTER INTERACTION : ENERGY DISSIPATION AND INJECTION LEVEL**

E. NAPCHAN

*Department of Materials Science, Imperial College of Science and Technology, GB-London, SW7 2BP, Great-Britain*

Résumé - La dissipation d'énergie d'un faisceau de lumière ou d'électrons dans un échantillon est le premier paramètre responsable de la génération des signaux utilisés pour la caractérisation de l'échantillon étudié. Les descriptions semi-empiriques du profil de dissipation d'énergie communément utilisées sont présentées. Leurs limitations dans le cas de conditions expérimentales particulières telles que les échantillons multicouches ou une variation de l'angle d'incidence du faisceau rendent nécessaires l'évaluation des paramètres d'interaction faisceau-matière par des méthodes telles que la simulation Monte-Carlo. Les principes physiques de ces simulations sont introduits et les détails d'un programme de calcul rapide développé par l'auteur sont donnés, concernant particulièrement l'évaluation de l'énergie déposée. Certaines applications de ces calculs, ainsi que d'autres, pour la caractérisation des propriétés des dispositifs par faisceau sont esquissées et des exemples de résultats de simulation sont comparés avec les données expérimentales.

Abstract - Energy dissipation by a light or electron beam inside a specimen is the primary parameter responsible for generating signals used to characterize the sample under investigation. The commonly used semi-empirical descriptions of this energy dissipation profile are presented. Their limitations in dealing with particular experimental conditions, such as multi-layer specimens and varying beam tilt angles, make it necessary to evaluate the beam-matter interaction parameters by methods such as Monte Carlo simulations. The physical principles of these simulations are introduced along with the presentation of computational details of a fast calculation program developed by the author, in particular for dealing with the evaluation of energy deposition. Some of the applications of calculated energy dissipation profiles and other data calculated in the beam induced assessment of device properties are outlined, along with examples comparing simulation results to experimental data.

## 1 - INTRODUCTION

Many physical phenomena caused by the interaction of a probing beam with a solid target material depend on the beam energy dissipation. Whether the purpose of the experiment is to study defects in a specimen, or to characterize physical properties, energy dissipation is the link between the beam parameters and the measured signals (e.g., charge collection current, cathodoluminescence light emission, x-ray generation, secondary and backscattered electron generation). In the general case the tri-dimensional energy dissipation per unit volume element is required, while in other circumstances it is possible to use two-dimensional representations which will be called energy doses. A further useful simplification is the use of the one-dimensional electron range.

Other intrinsic factors in research work with semiconducting materials relate to the actual specimens, their source and their availability. The specimens studied are usually in the form of completed, or almost finished devices. Their geometry can vary between production runs, either because of preparation conditions or from design changes. A great part of the work done is carried out for quality control, or failure analysis. Results of such research are usually required on a short time scale.

The energy dissipation of a probing electron-beam inside a solid target can be determined using empirical relations, mainframe Monte Carlo simulations of a large number of electron trajectories, or simplified Monte Carlo calculations run on micro-computers. The last approach will be presented in detail here. It satisfies the requirements for speed and flexibility with respect to specimen geometries, and can be easily adapted to almost any type of experimental situation. It will be shown that, in many instances, these methods are the only choice available.

The simulation is carried out on micro-computers, taking as input the specimen geometry and composition, and the beam parameters. The calculation is based on the Bethe energy loss relation and an empirically modified Rutherford relation for scattering of electrons. The results consist of a graphical display of electron trajectories, an energy dose plot, and a two dimensional matrix of energy deposition in the specimen. This last output is used for the evaluation of the required signals from the specimen, taking into consideration its electrical and structural (defect) characteristics.

Results from such Monte Carlo simulations and their comparison with experimentally evaluated data will be presented. These will include work with heterojunctions and Schottky diodes with non-negligible metal layers, and charge collection current evaluations from cross-sectional linescans.

For light probe excitation no such methods are available. With the increasing interest in techniques such as LBIC (light beam induced current) and PL studies, and with the increase in resolution of these techniques, it is possible that such methods will be developed.

The following paragraphs will introduce light beam and electron beam interactions with a solid sample from the point of view of modeling such interactions for further calculations of effects related to the beam dissipation of energy in the specimen. The development of such models for electron beams is better known to the author, and most of what follows will deal with this.

### 1.1 Light beams

Light beams can have advantages in relation to an electron beam for the investigation of semiconducting devices: no surface contamination, samples do not need to be observed in vacuum, no charging effects on the specimen surface, no charging of oxide layers for low energy photons

The spatial resolution obtained with light beams depends on the beam diameter (diffraction limited) at the focusing point in the sample. For wavelengths in the range 0.4 to 1.06  $\mu\text{m}$ , the focused spot size can vary between 2 and 0.3  $\mu\text{m}$ , and the corresponding maximum penetration depth in silicon is 0.5 to 1000  $\mu\text{m}$  /1/.

For a light beam of negligible cross section the depth distribution of generation is given by:

$$\Lambda(z) = \alpha \cdot G \cdot (1 - R) \cdot e^{-\alpha z} \quad (1)$$

- $\alpha$  - absorption coefficient (function of wavelength)
- $z$  - is depth in the material
- $G$  - number of photons/sec just outside the sample surface
- $R$  - surface reflection coefficient

This expression is equivalent to the Everhart and Hoff depth dose function for electron beams (as presented later). Donolato /2/ developed a model for the characterization of beam induced currents from vertical grain boundaries in silicon, using the above light absorption relation and the Everhart and Hoff depth dose for electrons. His model shows the equivalence between the two beam injection methods. The light absorption coefficient  $\alpha$  is shown to play a similar role to the maximum range for electrons ( $L/R$  and  $\alpha \cdot L$ , where  $L$  is the diffusion length in bulk silicon).

For beams of finite size, focused deep in the sample, the above relation for the depth distribution is no longer valid. Some form of convolution with the physical beam shape will be needed to generate the actual energy deposition in the specimen. The absorption coefficient can vary strongly as a function of the semiconductor impurity concentration /3/.

A three-dimensional light intensity distribution inside a single absorbing medium for a beam focused on the specimen surface has been used in /4/ to calculate light beam induced currents in p-n junctions and Schottky barriers. The effects of light reflectance and transmittance for various light incidence conditions and for single and double layer optical coatings on GaAs have been evaluated in /5/. A possible combination of these two approaches would lead to a more complete treatment of light beam interaction with multi-layer specimens, as is done in Monte Carlo simulations of electron trajectories.

### 1.2 Electron beams

To characterize the interaction of an electron beam with a target material, it is necessary to consider the position and energy of each beam electron along its trajectory (which will provide information related to the beam, such as the backscattering coefficient), and, the total energy deposited by the beam in a unit volume in the specimen.

Electrons travelling through a target are subject to two types of scattering events: (1) elastic scattering in which the electron direction is changed but not its energy, and (2) inelastic events in which both the energy and the travel direction are changed. Inelastic scattering can further be classified as single scattering events, resulting from one-one electron interaction, and multiple-electron excitations, where the primary electron interacts collectively with the specimen electrons (see Reimer and Joy for extended definitions of scattering types and cross sections).

The deflection of primary electrons by the positive charge of the target atom nucleus results in the elastic scattering. This effect is responsible for the spread of primary electrons in the specimen, as described by the "pear shape" dissipation volume. Rutherford and Mott developed basic formulae giving cross sections that describe this type of scattering processes: the first provides a relatively simple analytical expression, while the second can only be tabulated.

Among the various processes that result in inelastic scattering are those responsible for: secondary electron emission, inner shell electron ionization, bremsstrahlung (due to the coulomb field of the atom), plasmon scattering (due to the coulomb field of the beam electrons). The combined effect of all inelastic scattering on energy absorption by the target can be treated by Bethe's law without knowing the detailed inelastic scattering processes.

Each type of scattering event can be described by a cross section, which is a measure of the probability of the scattering process occurring. From the cross section, it is possible to define a mean free path between events. Because only elastic scattering events contribute to direction changes in the primary electron trajectory, it is possible to relate the electron path between single scattering events to the elastic mean free path.

A complete picture of the energy dissipation volume requires a three dimensional matrix, where each cell relates to a physical element in the specimen and gives the total energy deposited by the electron beam. Such a description is necessary sometimes, but usually simpler methods can be used. Electron beam doses provide the amount of energy deposited in a infinitely large element, where one of the dimensions is made infinitely small. A further simplification can be made by using various electron ranges to provide an envelope picture of the beam dissipation, which can then be calculated as a constant inside the defined region.

The rate of primary electron energy loss in a direction normal to the specimen surface is referred to as the depth dose function. Similarly, the lateral dose function is the energy loss rate in a plane perpendicular to the sample surface. An additional energy dose can be defined for concentric cylindrical surfaces, having the axis normal to the specimen surface. This dose function is referred to here as the radial dose function. A further description of the various doses and the means to evaluate them by Monte Carlo simulations is presented in section 2.2.

Each energy dose function can be applied to particular investigations related to EBIC (electron beam induced current) microscopy. The depth dose is mostly used for junctions normal to the beam direction, the lateral dose for junctions normal to the specimen surface, and the radial dose can be used to study line defects whose direction is normal to the specimen surface.

The commonly available energy dose as an empirical relation is the depth dose. Three such models are further presented, along with some of the definitions of the relevant electron ranges. For semiconductor work with device-specimens, their application is limited, as they do not cater for multi-layer specimens, and do not consider beam orientation apart from normal. Nevertheless, in many cases, they have been found useful, e.g., in work with Schottky diodes and p-n junctions, where the metal contact layer thickness is small compared to other geometric parameters related to the beam energy dissipation.

### 1.3 Electron ranges

#### Grün /36/ (primary electron range)

This is defined by extrapolation to zero of the linear decrease in the depth dose function. The resulting relation for different materials and beam accelerating voltages is:

$$R_G = C \cdot E^k \quad (2)$$

C, k - constants that depend on the material  
E - electron beam accelerating voltage

for GaAs	C=4.89	k=1.7	(/9/, /10/)
for 5<Z<15 and 5<E<35	C=4.0	k=1.75	(/7/)

This is the most commonly used range definition used in conjunction with the various analytical depth dose functions. But, values in the literature do not provide an accurate description of all experimental results, even for the case of silicon, for example in /6/, where ranges twice as much as those given above are suggested.

#### Bohr-Bethe range (continuous slowing down approximation range)

This is the electron path length in the material, obtained by integration of the Bethe energy loss relationship ( $\int(ds/dE) \cdot dE$ ) between the initial beam energy and some small energy value designed to avoid a discontinuity in the energy loss relationship for  $E=0$ .

#### 1.4 Electron beam energy depth doses

##### Everhart and Hoff /7/ depth-dose function

This expression was determined by measuring the steady state EBIC current (10  $\mu\text{m}$  beam diameter) through an MOS (metal-oxide-semiconductor) structure consisting of a thin insulating layer of silicon dioxide (1500-3000 Å), sandwiched between a top aluminum contact (900-2500 Å) and a silicon substrate.

This is probably the most widely used depth dose function, due to its simplicity, Eq. 3:

$$\Lambda(y) = 0.60 + 6.21 \cdot y - 12.40 \cdot y^2 + 5.89 \cdot y^3 \quad (3)$$

where  $\Lambda(y)$  is the relative amount of energy deposited at the reduced penetration depth  $y$ , given by

$$y = \frac{z}{R_G} \quad (4)$$

where  $R_G$  is the Grün range, given by:

$$R_G = 4.0 \cdot E^{1.75} \quad [\mu\text{g}/\text{cm}^2] \quad (5)$$

both Eqs. being valid for  $10 < Z < 15$  and  $5 < E < 25$  keV. Despite the ranges for the depth dose given above, this expression has been used in the literature for almost all materials and under "today's" SEM operating conditions (1 - 40 keV).

##### Kanaya and Okayama /8/ depth dose

Based on the relationship between backscattering and energy dissipation, a diffusion model represented by a sphere whose centre is located at the maximum energy dissipation depth is proposed and with radius equal to the difference between the maximum range and the maximum energy dissipation depth. The original diffusion model by Orchard consists of a sphere with centre at the diffusion depth, and radius equal to the difference between the maximum range and this diffusion depth.

The various range parameters are based on the maximum range, as defined in Eq. 6 for relativistic electrons:

$$\rho R = \frac{2.76 \cdot 10^{-11} A E^{5/3}}{Z^{8/9}} \cdot \frac{(1 + 0.978 \cdot 10^{-6} E)^{5/3}}{(1 + 1.957 \cdot 10^{-6} E)^{4/3}} \quad (6)$$

The diffusion depth, defined as that for which the transmitted fraction of electrons is  $[1/e]$  is given by:

$$x_d = \frac{R}{1 + \gamma} \quad \text{with} \quad \gamma = 0.187 \cdot Z^{2/3} \quad (7)$$

The maximum energy dissipation is obtained as:

$$x_e = \frac{R \cdot (1 + 2\gamma - 0.21 \cdot \gamma^2)}{2(1 + \gamma)^2} \quad (8)$$

Energy dissipation per unit penetration depth is calculated based on the reduced depth,  $\gamma$  and an experimental value for the mean energy of backscattered electrons. This distribution when compared to available experimental data showed only qualitative agreement, with the peak value located at almost the same reduced depth.

Wu and Wittry depth dose function

The Wu and Wittry /9/ depth distribution function is a modification of the Gaussian approximation given by Kyser /34/. Normalization to the Grün range as in /10/ yielded Eq. 9 which was used for GaAs and GaAsP:

$$g(z) = 1.48 \cdot \left[ e^{-(1.77z - 0.36)^2} - 0.4 \cdot e^{-19.8z} \right] \quad (9)$$

$z$  - normalized depth defined by:  $z = \frac{Z}{R}$   
 $Z$  - depth in the material [ $\mu\text{m}$ ]  
 $R$  - range in [cm] defined by:

$$\rho \cdot R = 4.89 \cdot E^{1.7} \quad (10)$$

with  $\rho$  - density of material [ $\mu\text{gr}/\text{cm}^3$ ]

## 2 - MONTE CARLO SIMULATIONS

### 2.1 Methods

A recent review of the principles on which Monte Carlo simulations are based can be found in the work of Murata and Kyser /30/. This also includes details of calculations for specimens with mixed layers, and in particular, for organic materials (used in electron beam lithography) deposited on semiconducting materials.

The reasons for performing fast Monte Carlo simulations have been outlined in the introduction. There are various implementations of such procedures, each with its specific characteristics. The work reported by /11/ uses the Mott elastic cross section, at the expense of calculation time, to simulate more precisely interactions with low accelerating voltage electron beams. Other programs /12/ were used for studies of grain boundary segregation in the analytical electron microscope.

The Monte Carlo programs used here originated from the programs written by Joy, /13/, /14/, /15/. These were modified by the present author to include analysis of multi-layer samples and to provide data about energy dissipation volumes. An important aspect in the development of these programs was to make their use available to interested workers who want to obtain numerical data for use in charge collection calculations which can not be obtained by simple analytical expressions without some uncertain approximations.

### 2.2 Description of PC-MCS (personal computer Monte Carlo Simulation)

#### Specimen description

The specimen geometry can consist of almost any number of different layers, in any combination. The coordinate system used has the  $z$ -axis pointing downward and the  $y$ -axis horizontal, increasing to the right. The coordinate  $R$  is defined as the radial distance of a point from the  $z$  axis. The beam is fixed at  $z=0$ ,  $y=0$ ,  $x=0$ , and the top surface of the specimen is  $z=0$ . The initial beam incidence point is fixed at position  $x=z=y=0$ , but its direction of tilt can be defined with relation to the specimen surface. Experimentally, the sample would have to be tilted to the required angle.

Only the  $y$  and  $z$  coordinates are input for defining the geometry of the sample (assuming symmetry along the  $x$  axis), although the calculations of electron positions inside the specimen are carried out in three dimensions. The evaluation of energy deposition density and charge collection current is carried out in two dimensions only, as described in the next section.

#### Material properties required

The material properties required to perform the simulation are: atomic number, atomic mass and density. For specimens of mixed elements the values used for the atomic number and mass are the atomic mass weighted averages of those of the elements in the compound. This assumption was used by Kyser (1979) for his calculations of step lengths in composite materials for Monte Carlo simulations. Bresse /33/ also used a weighted average of atomic weights and atomic numbers to calculate mean parameters for use with the Everhart and Hoff depth dose function.

#### Elastic scattering treatment

The calculation of the electron trajectory uses a screened Rutherford cross section to evaluate the elastic scattering angle. This angle is based on the NBS /16/ modifications to the expression given by Curgenvin and Duncumb for the Rutherford original elastic scattering cross section. The azimuthal scattering angle for each scattering event is found by assuming that an electron can scatter with equal probability to any point in the plane normal to the direction of the original incidence direction.

Two random numbers, generated independently, are used to evaluate the scattering angles. From these the simulation derives its name: Monte Carlo!

#### Inelastic scattering and step length

The Bethe continuous energy loss relation represents the inelastic scattering and gives the energy deposited along each trajectory step for each electron. The small trajectory deviations due to the inelastic scattering are neglected. The value required for the mean ionization potential in Bethe's expression is calculated from the Berger and Seltzer relation (see for example /17/ for alternative forms of evaluation).

The primary electron step length and energy loss profile are calculated from the integral of the Bethe equation. The step length is constant and equals 1/50th of the calculated Bethe range.

#### Electron transport across boundaries

A problem in simulating transport in multi-layer specimens is how to handle electron transport across boundaries of different layers. A first approximation used in this work is to change the electron scattering and beam stopping parameters after crossing the boundary, without evaluating precisely the partial electron step length in each of the layers. Inaccuracies are introduced at this type of crossover, which can result in errors in the energy deposited. But, when considering the average of many electron trajectories, and that the dose inside each layer is "correctly" evaluated, these errors can be reduced by smoothing the results. An additional approximation is made in the case of transport across material boundaries, in that no special attention is given to boundary conditions, e.g., impurity segregation and structural defects.

#### Energy deposition calculation

The electron positions along the trajectory are calculated using the geometrical equations derived by /16/, /35/ with the above defined scattering angles, energy-loss relation, and step lengths for each different layer.

The energy deposited in the specimen for each step in the trajectory of each primary electron is equally distributed between two points along the trajectory step. This results in increased "resolution" of the energy deposition function compared to the step length used in the simulation, and was found to be necessary in cases where the electron step is of the same order of magnitude as one of the geometrical dimensions of the specimen. Energy deposition data is stored in an 80 by 80 matrix for a geometric volume of dimensions input at the beginning of the simulation (called llz in the programs). Usually, this value in the z direction corresponds to the expected penetration range, and in the radial direction the same value is used. If, at any step along their trajectory, electrons move to positions outside this region (or outside the sample geometry), their remaining energy is summed up in a value designated as out-energy, which defines the amount of energy not included in the energy deposition array or in the backscattered energy. The backscattered energy is calculated by summing the 'leaving' energy of electrons emitted from the specimen through the top surface.

The electron trajectories are calculated in three dimensions, but the resultant energy deposition profiles are stored in a two-dimensional matrix. Two types of matrix can be used to store the energy deposition values: (i) for horizontal annular sections for each depth, and, (ii) for horizontal lateral stripes for each depth. Fig. 1 presents the two methods for storing energy deposition data. In this figure, only one layer section is presented. The width and relative position of each section in this layer, with respect to the beam incidence point, is given in units of llz, as defined above.

The annular sections matrix gives the energy deposited on each plane perpendicular to the beam direction and in circular rings around the point of beam incidence. Because of the radial symmetry of the energy dissipation volume (for normal beam incidence) these rings constitute areas of constant energy deposition. This type of energy matrix allows for the reconstruction of the three dimensional energy beam deposition density and also allows the calculation of the various possible dose functions. It is also convenient when the energy inside cylindrical surfaces around the beam direction is needed, as in the evaluation of charge collection for line defects normal to the sample surface.

The lateral stripe distribution as a function of depth does not allow the reconstruction of the three dimensional energy distribution. It was found useful for calculations where the charge collection barrier is parallel to the incident beam direction /18/ and for studies of line defects normal to the incident beam direction.

From the annular matrix distribution it is possible to reconstruct the three dimensional energy distribution per unit volume (for normal beam incidence angle), and to evaluate the above dose functions. From the lateral stripes matrix only the depth and the lateral dose functions can be evaluated, the later requiring simple summations compared to the calculations required for the annular matrix distribution.

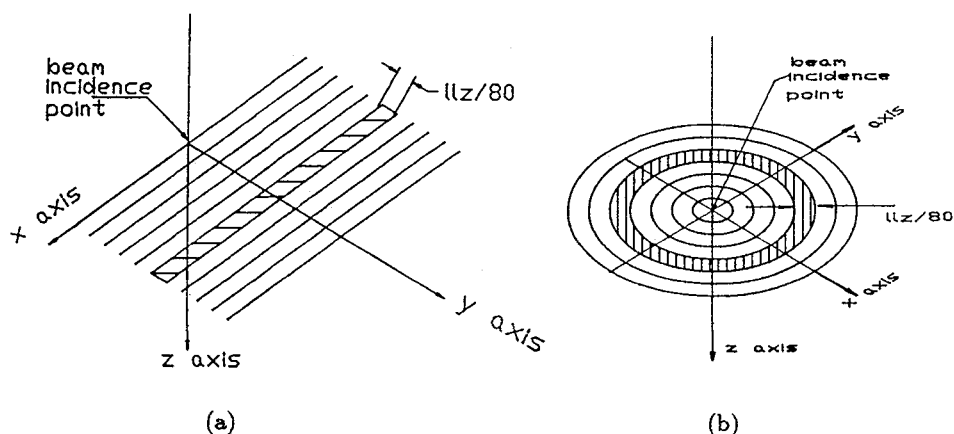


Fig. 1 - Definition of energy deposition sections used in the Monte Carlo simulation output: (a) lateral stripe element, (b) annular section element.

#### Data output

The data produced by the simulation is displayed on the computer screen (or printed) as a picture of electron trajectories in the sample, along with a plot of the depth dose, and data about the overall energy losses by the beam (see Fig. 3). In addition, the energy deposition matrix selected, as described previously, is stored on disk for further calculations. Typical running time for a simulation is one electron trajectory calculated per second, with relatively smooth data obtained for simulations of 2000 electrons.

### 3 - USING MONTE CARLO SIMULATION DATA

#### 3.1 Charge collection microscopy (OBIC and EBIC)

Changes in the depth dose functions as a result of electron beam energy absorbed in a metal contact layer modify the EBIC current predicted from a device. Fig. 2 presents ratios of the CCC (for a range of beam voltages) calculated for Schottky Au/Si diodes with varying thicknesses of gold, compared to the theoretical current for a diode with a negligibly thin gold layer. The calculations were done for a Si diffusion length of  $25 \mu\text{m}$ , which makes the results sensitive to the total energy deposited but less so to the shape of the depth dose function.

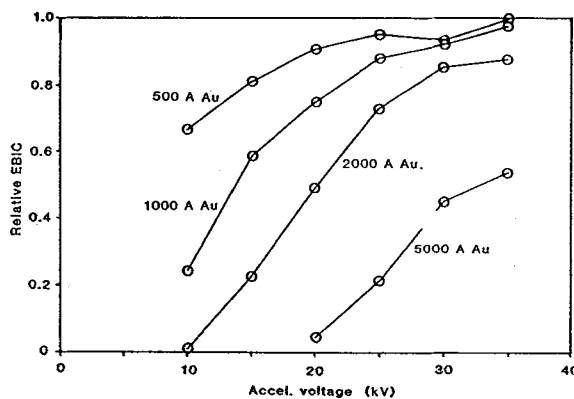


Fig. 2 - Ratio of EBIC current for Au/Si junctions as function of gold thickness

It can be seen that a gold layer of as little as 500 Å reduces the total current considerably, this reduction being greater for lower accelerating voltages. The change is more significant for lower accelerating voltages because a larger fraction of the energy gets absorbed in the gold layer.

If the Schottky metal layer has thickness variations (e.g. pin-holes or hillocks), these will appear as variations (contrast) in the EBIC signal. These variations in contrast may not be observed in the secondary electron image of the SEM. For a 20 kV beam and a 1000 Å gold film, variations of  $\pm 500$  Å will change the EBIC current by about 30 %. This strong EBIC contrast might be misinterpreted as resulting from some defect in the semiconductor.

### 3.2 Composition based on backscattered electrons

The backscattered electron signal is one of the least used in SEM microscopy, despite the fact that detectors are available "built-in" on some microscopes. One of the checks carried out with Monte Carlo simulations is the evaluation of backscattering coefficients for different materials and beam tilt angles. The programs described here were tested by comparing their backscattered coefficient results to experimental data (as a function of atomic number at 30 kVolts, /17/, and as a function of beam tilt angles for iron at 25 kV, /16/). In both cases, a good quantitative fit was obtained.

The use of Monte Carlo simulations for obtaining backscattered data (not for comparison purposes) is not common. A recent report, /19/, presented the use of backscattered electron signal in the study of epitaxial multi-layer structures of Cadmium Mercury Telluride on Cadmium Telluride. Fine scale compositional variations (with a spatial resolution better than 0.1  $\mu\text{m}$ ) were experimentally measured using the backscattered signal after image processing. The shape of this backscattered signal linescan was interpreted using Monte Carlo simulations, and a good quantitative agreement was attained.

An anomalous inversion in the backscattered electron contrast has been observed in an aluminum-silicon eutectic alloy when the beam accelerating voltage is increased above 20 kVolts, /20/. It is well known, /21/ and /17/, that the backscattered electron energy spectra can vary as a function of atomic number and beam energy. By calculating the energy spectra of backscattered electrons using Monte Carlo methods, and combining this with the detector response, it might be possible to obtain a better understanding of this effect.

For specimens composed of different layers the backscattering coefficient can vary depending on the beam conditions (angle and voltage). The following tables present calculated data for the variation of backscattering coefficient and energy for two types of specimens. This contrasts with single materials for which the backscattering parameters remain approximately constant over similar beam voltage ranges.

Table 1 - Backscatter data for gold on silicon (calc. by Monte Carlo simulation)

Au thick.	500 Å		1000 Å		2000 Å		5000 Å	
	$\eta$	$E_\eta$	$\eta$	$E_\eta$	$\eta$	$E_\eta$	$\eta$	$E_\eta$
10	.40	.31	.47	.35	.47	.35	-	-
15	.33	.26	.41	.31	.44	.33	-	-
20	.28	.21	.34	.27	.43	.33	.46	.35
25	.23	.18	.28	.23	.38	.30	.45	.34
30	.24	.19	.27	.21	.33	.26	.43	.32
35	.18	.13	.21	.16	.30	.24	.43	.33

Table 2 - Backscatter data for CdTe/Si heterojunctions (calc. by Monte Carlo simulation)

Structure	1		2		3		4	
	$\eta$	$E_\eta$	$\eta$	$E_\eta$	$\eta$	$E_\eta$	$\eta$	$E_\eta$
	Calculated values		Calculated values		Calculated values		Calculated values	
Voigt [kV]								
7	.38	.27	.39	.28	.40	.28	.40	.27
10	.36	.27	.38	.26	.39	.27	.38	.26
15	.28	.21	.37	.27	.28	.28	.39	.28
20	.23	.17	.29	.22	.37	.28	.38	.27
25	.21	.16	.28	.21	.32	.25	.35	.26
30	-	-	.25	.18	.28	.22	.31	.24

Structure type: 1 - 1500 Å CdTe on Si  
 2 - 3000 Å CdTe on Si  
 3 - 1500 Å In on 3000 Å CdTe on Si  
 4 - 3000 Å In on 3000 Å CdTe on Si

### 3.3 X-ray intensities

Monte Carlo results were at first used for the analysis of EPMA data, in particular X-Ray generation. When the specimen is a mixed target, or composed of different layers, these methods are uniquely used for the derivation of compositional information with spatial resolution. Two recent applications of simulations in this field are presented.

ZAF (atomic number, absorption and fluorescence) corrections in X-Ray microanalysis were extended to deal with tilted specimens /22/, by using simulation data and tracer experiments. This should increase the scope of the technique by allowing a greater sensitivity to surface regions.

Based on Monte Carlo programs for the evaluation of X-Ray intensities Armigliato et al. /31/ have measured oxygen contents in polycrystalline silicon, determined layer thicknesses in multi-layer specimens, and calculated beam tilt conditions necessary to achieve the required composition resolution.

## 4 - EXPERIMENTAL USES OF MONTE CARLO SIMULATIONS

### 4.1 Multi-layer devices

Fig. 3 presents the calculated depth dose function for a CdTe/Si heterojunction, for a beam accelerating voltage of 10 kVolts. It can be seen that the transition from the CdTe to the Si substrate in the energy dose is not a smooth one, and therefore could not be obtained by means other than Monte Carlo simulations. These calculated depth dose functions were used in the determination of the diffusion length in the CdTe, and for the determination of the thickness of a In contact layer deposited on the CdTe /23/. In the second example, the best fit was compared to the measured thickness obtained by a moving style measurement, and good agreement was found.

Experimental charge collection investigation of heterojunction samples at a particular beam voltage resulted in EBIC intensity from the contact layer stronger than that from the bare semiconductor. This led to the proposition of a rectifying contact barrier, with stronger rectification than the actual heterojunction under consideration. When investigating at different beam voltages, it was found that the relative amount of contrast changes and undergoes an inversion in which the signal from the semiconductor becomes the strongest.

This effect was investigated by running Monte Carlo simulations for the same devices. The result of these simulations is presented in Fig. 4, in which the ratio between the charge collection currents measured from the metal contact and at the top semiconductor changes sign, reflecting the experimentally observed contrast inversion. Other mechanisms could be responsible for the same type of effect, e.g., changes in the CdTe doping density as a result of In diffusion. A definitive answer to the reasons for this observation needs additional investigation.

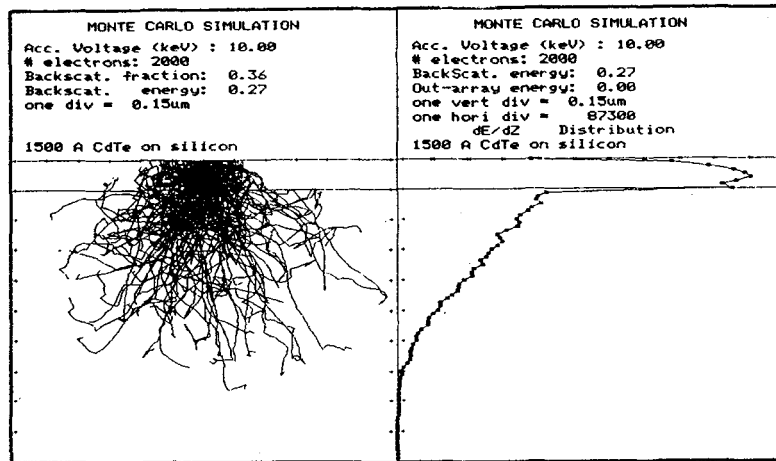


Fig. 3 - Depth dose function and electron trajectories for an heterojunction (1500 Å CdTe on a Silicon substrate, at 10 kVolts beam energy)

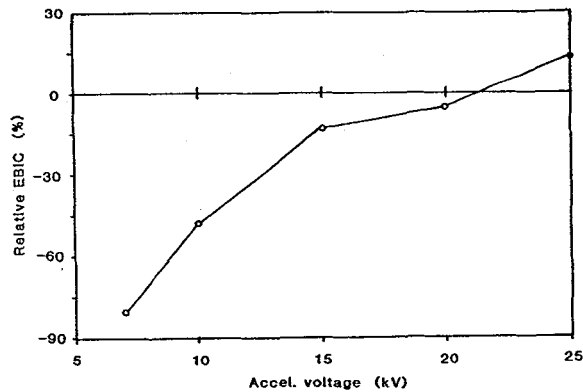


Fig. 4 - Calculated contrast for a layered structure (3000 In on 3000 CdTe on Si substrate)

From the variation in the charge collection current with beam voltage, it is possible to determine geometric parameters of the specimen constituent layers, when the electrical parameters are known. By running simulations for different values of thickness, it was possible to fit the calculated data to the EBIC measurements (in /24/ for Schottky diodes, and /23/ for CdTe/Si heterojunctions) and obtain the best fit value. The value was then compared with experimentally measured thickness values, and in all cases a good correlation was found. Fig. 5 presents such results described in /24/.

#### 4.2 Cross-section work

##### Linescans on Si p-n junctions

Hungerford /18/ reported experimental work related to the characterization of the shape of EBIC linescans for p-n junctions. The experimental conditions used were: high magnification of cross-sections of silicon p-n junctions, at various reverse bias values, and for beam voltages up to 20 Volts. Fig. 6 shows the sample configuration and the experimental results obtained for a 25 kVolts beam, for different reverse bias values applied to the specimen. The analysis of this type of experimental data was carried out by extending the Donolato theory /25/ with an original lateral generation function. This function was calculated from the lateral energy dissipation matrix obtained by the MCS program, and gave 80 horizontal lines of energy dissipation located at a depth of  $0.3 \cdot R$  ( $R$ -Grün range). For each beam position along the p-n junction cross section, the EBIC current was calculated for all 80 values of the generation function. This calculation took into consideration the following parameters: the depletion region width and diffusion lengths on both sides of the junction, surface recombination effects, and in some cases carrier recombination inside the depletion region. For beam voltages higher than 15 kVolts, under all bias conditions investigated, the fit between experimental linescans and calculated ones was very good, as shown in Fig. 6.

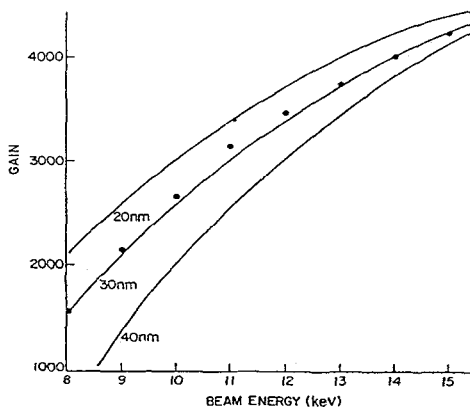


Fig. 5 - Use of Monte Carlo simulations for the estimation of metal layer thickness /24/

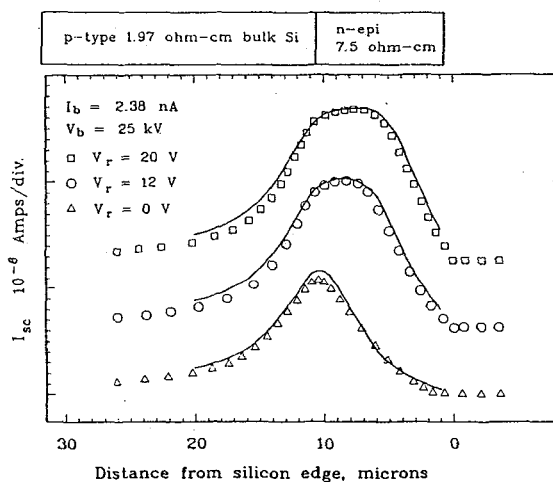


Fig. 6 - EBIC linescans in p-n junctions cross sections and fit to model using the lateral generation function from the PC-MCS programs (from /18/)

One of the suggestions in /18/ for extending the analysis of this type of experimental EBIC data, for example for lower beam voltages, was to use the full lateral energy dissipation matrix, as calculated by the PC-MCS program. The only limitation for doing this is the required computational time: the time ratio between the approach used and the full use of the energy deposition matrix (80 lines, or 6400 matrix elements) would be about 80. This computation time increase was considered unrealistic for the total amount of data that would have to be evaluated.

#### GaAs structures

Akamatsu et. al. (1981) measured diffusion length in GaAs for cross sections of Schottky diodes and p-n junctions taking into consideration the effect of surface recombination, and of reabsorbed radiative recombination radiation ("RRR", generation of electron-hole pairs by the CL [cathodoluminescence] emission absorption in the specimen). In their work they used the 3-dimensional energy distribution, and also calculated the lateral dose. In the context of the programs presented here, the lateral stripes energy distribution matrix could be used for the calculations, due to the symmetry of the problems studied (vertical collecting junction and horizontal surface where additional recombination takes place).

Another interesting result presented in this work reflects the fact that the EBIC method must be carefully used to locate accurately the position of the p-n junction: for different diffusion length values the peak position in the calculated linescan profile varies, depending on the ratio between the diffusion lengths and the beam accelerating voltage.

#### 4.4 Study of defects

Apart from the description of the sample geometry and the experimental conditions, the study of defects requires some input with respect to the interaction between the electron beam energy dissipation volume and the defect. Various physical/empirical relations can be used, depending on our knowledge about the defect under study and the particular model one wishes to use.

Asymmetrical EBIC profiles were found when scanning across vertical grain boundaries in GaP in /26/. These were modeled as two Schottky barriers back to back, with different barrier height and bulk minority carrier diffusion lengths on both sides of the boundary. Charge collection micrographs showed a bright-dark contrast when crossing the boundary, which could be made either dark or bright by applying an external bias across the boundary.

Monte Carlo simulations were used to generate the lateral dose function with a view to calculating charge collection currents for such a system. As a first approximation, the electrical parameters considered were the diffusion lengths in the grains and the width of depletion region in each side of the boundary. In this model, the interface between the two grains is assumed to be negligibly thin and not to affect the electron trajectories as they cross from one grain to another. As the sample is believed to have a small minority carrier diffusion length compared to the generation volume, the point source generation and the uniform generation sphere model could be inaccurate at least for certain ranges of beam accelerating voltage. Although lower beam voltages would reduce the dissipation volume, the results then are more likely to be prone to surface effects.

Fig. 7(a) presents linear and log-linear plots of the lateral and depth doses calculated for GaP and a beam voltage of 15 kV. Fig. 7(b) shows some simulated EBIC profiles calculated for the lateral dose in (a), for the boundary model described above. These give a good qualitative fit to data presented in /26/. As always, when fitting data calculated from simulations with a large number of variables to experimental data, more results are needed to fully characterize the phenomena.

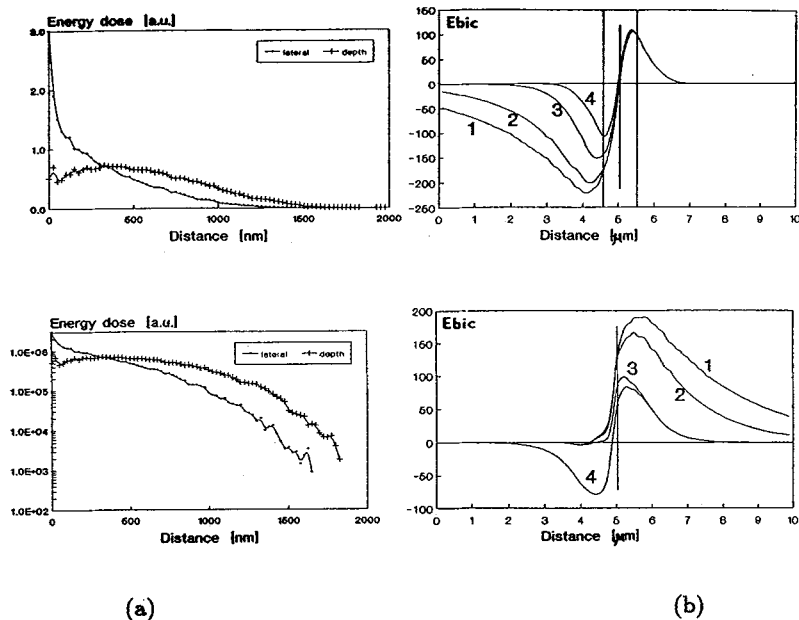


Fig. 7 - Studies of GaP grain boundary

a) linear and log-linear plots of calculated electron beam depth and lateral doses, for a beam voltage of 15 kVolts

b) simulated EBIC profiles for linescans using the lateral dose presented in a). For the top Fig.7(b) the values assumed for the depletion widths were  $0.5 \mu\text{m}$  on each side, and for the diffusion lengths on the r.h.s. was  $0.1 \mu\text{m}$  and for the l.h.s were: 1-  $2.5 \mu\text{m}$ , 2-  $1.5 \mu\text{m}$ , 3-  $0.5 \mu\text{m}$  and 4-  $0.1 \mu\text{m}$ . For the bottom of Fig. 7(b), the corresponding values were:  $0.1$  and  $0.1 \mu\text{m}$  for the depletion widths, and the same values as before for the diffusion lengths.

The shape of the depth and lateral dose functions presented in Fig. 7 agrees well with that given in /3/, which was also calculated by Monte Carlo simulations. In addition, the lateral dose linear-log plot also agrees with that calculated in /32/ from Grün's data for penetration of electrons in air.

#### 4.5 Future applications

##### Monte Carlo simulations of charging effect

Additional negative charge will occur in a SEM specimen when it is not capable of conducting to ground electrons due to the beam and due to the secondary electron generation. When working with semi-insulating or insulating materials, this effect is commonly observed as a high secondary electron signal (bright contrast), and in some cases, sudden discharges.

In addition to visual effects, specimen charging also induces changes in other measurable quantities such as beam induced currents, and in some cases, can also damage the specimen under observation. In electron beam lithography, when insulating organic layers are scanned by an electron beam, the changes in the beam energy dissipation profiles can have a significant effect on the resolution attained. Studies of MOS structures, carried out at low beam accelerating voltages are typical examples where beam exposure can damage the device's electrical characteristics by inducing charge in the gate oxide layer and causing undesired shifts in the current voltage characteristics.

A first approach to the evaluation of the dependence of charging on the various parameters related to the interaction of an electron beam with an insulating layer has been recently made by Kotera and Suga /27/. This study conducted Monte Carlo simulations of electron trajectories, assuming a fixed potential (charge) distribution in a thick PMMA layer (electron resist used in electron beam lithography), both when the top specimen surface is grounded and when it is left floating. Their work quantifies changes in beam energy dissipation volume and in backscattering coefficients for both above conditions. Further work needs to be done to take into account various influences not yet considered: the time dependent charge distribution, electron beam induced conduction, secondary electron emission, etc, to make this type of result applicable to studies of semiconducting/insulating devices.

##### Injection levels

The injection level refers generally to the ratio between the density of the beam generated carriers and the local equilibrium carrier concentration. When the excess carrier density is much smaller than the local doping, the injection conditions are low level. Intermediate injection levels have been suggested to be responsible for reduced junction collection efficiencies and changes in the measured minority carrier diffusion lengths /28/, and more so when these are considered under high surface recombination velocities /29/.

Most beam induced current studies do not consider the variations in local injection levels. It is only when increasing beam powers result in significantly different results that the injection level is considered, and then, usually by considering the beam as a point generation source, located at some distance beneath the specimen surface. Cathodoluminescence and X-Ray studies are cases in which high-injection conditions may be necessary for the generation of detectable signals, and they are usually associated with high beam powers.

In the uniform sphere generation model of beam dissipation the excess carrier generation level is assumed to be constant throughout. From Fig. 7(b) it can be seen that because both depth and lateral dose function are highly asymmetrical this is far from a true representation.

An approximate estimate for accessing the density of injected carriers for a uniform generation sphere model of beam energy dissipation volume is given by /29/. To generalise the application of this model to any generation distribution it is suggested to sum up the effects of infinitesimal sphere-point sources by considering some "average" equivalent radius and "average" distance from the surface.

Using Monte Carlo simulations it is possible to define the local excess carrier generation levels with a view to calculate where high injection conditions prevail. This can be carried out by several methods, using a combination of the depth, lateral and radial dose functions. For an accurate evaluation of the high injection volume, the full three dimensional beam dissipation has to be mapped as iso-energy plots, similar to the contours of equal luminous intensity induced by an electron beam incident on air (the familiar "pear shaped curves") as presented in the work of Grün, or to the electron-beam resist cross-sections obtained in lithography work. This will precisely define the variation in beam generation levels.

##### Beam tilting experiments

Changing the beam angle of incidence provides a controlled way of varying the depth profile of the beam interaction volume with the specimen. Monte Carlo methods are unique in their application to

these conditions, since the other analytical methods assume, by definition, a normal beam incidence angle.

Applications to this type of experiments was described already in the sections dealing with composition and layer thickness determination using the backscattered and X-Ray signals. A further use for this technique is described in /24/, in the study of small regions of semiconducting materials. By using the SEM beam rocking mode of operation /37/, while keeping the beam fixed on a small selected area, EBIC profiles as a function of tilt angle and beam accelerating voltage can be easily obtained. This data can be fitted to models describing the device's electrical behaviour, and quick estimates of the local minority carrier diffusion length and depletion width can be made (see for example the simulated linescans in /24/).

When thin semiconducting layers are deposited on thick substrates (e.g. in thin film heterojunctions) with large diffusion lengths, it is difficult to measure their electrical properties, as most of the signal comes from the substrate. Measurement of EBIC as a function of beam tilt angle can provide additional experimental data which when combined with simulation results will allow better evaluation of the thin layer materials.

## REFERENCES

- / 1/ WILSON T., OSICKI W. R., GANNAWAY J. N and G. R. BOOKER G. R., J. Mater. Sci. 14 (1979) 961-965
- / 2/ DONOLATO C., J. Appl. Phys. 54 (1983) 1314-1322
- / 3/ AKAMATSU B., HENOC J. and HENOC P., J. Appl. Phys. 52 (1981) 7245-7250
- / 4/ WILSON T. and PESTER P. D., IEEE Trans. Electron. Devices ED-34 (1987) 1564-1570
- / 5/ ARORA N. D. and HAUSER J. R., J. Appl. Phys. 53 (1982) 8839-8845
- / 6/ MAREK J., J. Appl. Phys. 53 (1982)
- / 7/ EVERHART T. E. and HOFF P. H., J. Appl. Phys. 42 (1971) 5837-5846
- / 8/ KANAYA and S. OKAYAMA S., J. Phys. D 5, 43-58
- / 9/ WU C. J. and WITTRY D. B., J. Appl. Phys. 49 (1978) 2827-2836
- /10/ PIETZSCH J., Solid-St. Electron. 25 (1982) 295-304
- /11/ REIMER L. and STELTER D., Scanning 8 (1986) 265-277
- /12/ MICHAEL J. R., CLIFF G. and WILLIAMS D. B., Scanning Electron Microscopy 1984-V 4161 (SEM Inc., AMF O'Hare, Chicago USA)
- /13/ JOY D. C., 40th Ann. Proc. Elect. Micros. Soc. Amer. (1982), (ed. G. W. Bailey), Claitors Publishing Division, Baton Rouge LA USA
- /14/ JOY D. C., Bell Labs. Technical Memorandum TM-82-11521-35 (1982)
- /15/ JOY D. C. and PIMENTEL C. A., Microscopy of Semiconducting Materials 1983, Conf. Series No. 68 (Inst. Phys.: Bristol) 355-360
- /16/ MYKLEBUST R. L., NEWBURY D. E. and YAKOWITZ H., "Use of Monte Carlo Calculations in EPMA and SEM" (1976) 105-128, (ed. K. F. J. Heinrich et al.) NBS Special Publication 460
- /17/ REIMER L., "Scanning Electron Microscopy", pub. Springer-Verlag, Berlin Heidelberg (1985)
- /18/ HUNGERFORD G. A., Ph. D. Thesis 1988 University of London
- /19/ LYSTER M. and BOOKER G. R., Electron Microscopy and Analysis 1987, Conf. Series No. 90 (Inst. Phys.: Bristol) 197-200
- /20/ BALL M. D., WILSON L. and WHITMARSH S., Electron Microscopy and Analysis 1987, Conf. Series No. 90 (Inst. Phys.: Bristol) 185-188
- /21/ DARLINGTON E. H. and COSSLETT V. E., J. Phys. D: Appl. Phys. 5 (1972) 1969-1981
- /22/ LOVE G. and SCOTT V. D., Electron Microscopy and Analysis 1987, Conf. Series No. 90 (Inst. Phys.: Bristol) 353-356
- /23/ NAPCHAN E. and HOLT D. B., Microscopy of Semiconducting Materials 1987. Conf. Series No. 90 (Inst. Phys.: Bristol) 733-738
- /24/ JOY D. C., J. Microsc. 143 (1986), 233-248
- /25/ DONOLATO C., Solid-St. Electron. 25 (1982) 1077-1081
- /26/ ZIEGLER E., SIEGEL W., BLUMTRITT H. and BREITENSTEIN O., phys. stat. sol. (a) 72 (1982) 593-605
- /27/ KOTERA M. and SUGA H., J. Appl. Phys. 63 (1988) 261-268
- /28/ DAVIDSON S. M., INNES R. M. and LINDSAY S. M., Solid-St. Electron. 25 (1982) 261-272
- /29/ BERZ F. and KUIKEN H. K., Solid-St. Electron. 19 (1976) 437-445
- /30/ MURATA K. and D. F. KYSER D.F., Adv. Electronics and Electron Phys., (P. W. Hawkes - editor) 69 (1987) 176-259
- /31/ ARMIGLIATO A., DESALVO A., GARULL A. and Rosa R., Microscopy of Semiconducting Materials 1981. Conf. Series No. 60 (Inst. Phys.: Bristol) 237-242

- /32/ SHEA S. P., PARTAIN L. D. and WARTER P. J., Scanning Electron Microscopy 1978-I 435-442 (SEM Inc., AMF O'Hare, Chicago USA)
- /33/ BRESSE J. F., Scanning Electron Microscopy 1982-IV 1487-1500, (SEM Inc., AMF O'Hare, Chicago USA)
- /34/ KYSER D. F., Chap. 6 in "Monte Carlo Simulation in Analytical Electron Microscopy" 1979, (eds. J. J. Hren, J. I. Goldstein and D. C. Joy), Plenum Press New York
- /35/ NEWBURY D. E. and MYKLEBUST R. L., in "Analytical Electron Microscopy -1981" 91-98, (ed. R. H. Geiss), San Francisco Press CA, USA
- /36/ GRÜN A. E., Z. Naturforsch. 12A (1957)
- /37/ JACUBOWICZ A., Solid-St. Electron. 25 651